Effect of carbon contamination on the printing performance of extreme ultraviolet masks

Yu-Jen Fan,[a] Leonid Yankulin, Alin Antohe, Petros Thomas, Chimaobi Mbanaso, Rashi Garg, and Yunfei Wang
College of Nanoscale Science and Engineering, University at Albany, Albany, New York 12203

Andrea Wüest, Frank Goodwin, and Sungmin Huh
SEMATECH, Albany, New York 12203

Patrick Naulleau, Kenneth Goldberg, and Iacopo Mochi
Center for X-Ray Optics, Lawrence Berkeley National Laboratory, Berkeley, California 94720

Gregory Denbeaux
College of Nanoscale Science and Engineering, University at Albany, Albany, New York 12203

(Received 10 November 2009; accepted 2 February 2010; published 22 March 2010)

Carbon contamination is a significant issue with extreme ultraviolet (EUV) masks because it lowers throughput and has potential effects on imaging performance. Current carbon contamination research is primarily focused on the lifetime of the multilayer surfaces, determined by reflectivity loss and reduced throughput in EUV exposure tools. However, contamination on patterned EUV masks can cause additional effects on absorbing features and can affect the printed images. In this work, various carbon contamination experiments were performed to study the impact between contamination topography and observed imaging performance. Lithographic simulation using calculated aerial images and experimentally determined resist parameters was performed and compared to the printing results to estimate the allowed carbon thickness with critical dimension compensation applied to the mask. © *2010 American Vacuum Society.* [DOI: 10.1116/1.3333434]

I. INTRODUCTION

Carbon contamination of extreme ultraviolet (EUV) masks, which is due to the photoinduced chemical reaction of residual hydrocarbons and EUV photons on the mask surface, is one of the critical issues hampering the introduction of EUV lithography into high-volume manufacturing (HVM). To investigate the impact of carbon contamination on the imaging of EUV masks, an EUV mask was intentionally contaminated at the College of Nanoscale Science and Engineering (CNSE) at the University at Albany and analyzed before and after contamination using several techniques. Additionally, lithographic simulation was performed to assess the contamination topography, estimate the allowed carbon thickness, and determine critical dimension (CD) compensation strategies to mitigate the effects of carbon contamination.

The EUV microscope for mask imaging and contamination study (MiMICS) tool was built at CNSE.[1,2] It is equipped with an Energetiq EQ-10M xenon-based discharge-produced plasma source[3] and a gas injection system to introduce carbon-containing molecules into the vacuum chamber. The MiMICS tool thus enables controlled contamination of an EUV mask by selecting a set of experimental parameters, namely, contaminant species, partial pressure, and most importantly, EUV dose.

A patterned EUV mask was inspected using a reticle scanning electron microscope (SEM), the SEMATECH Berkeley actinic inspection tool (AIT),[4] and an atomic force microscope (AFM). In addition, wafers were printed with the mask at EUV exposure tool using the SEMATECH Berkeley microfield exposure tool (MET),[5] which were then inspected with a CD-SEM.

Lithographic simulations were performed based on the printing results to understand the contamination topography on EUV masks. Using previously determined resist parameters, aerial images were calculated and compared to the experimental data. The simulated results of contamination topography were used to predict allowed carbon thickness with optical correction applied on the mask.

II. SYSTEM OVERVIEW

A schematic of the EUV MiMICS tool is shown in Fig. 1. This tool was designed to study the effects of carbon contamination on imaging performance of EUV masks. It is equipped with an Energetiq EQ-10M xenon-based discharge-produced plasma EUV source. In general a Si/Zr filter blocks wavelengths longer than approximately 18 nm, and also works well to separate the exposure vacuum chamber from the source. To increase local partial pressures and accelerate carbon deposition to a level allowing experiments to be performed within a reasonable time frame, the incoming beam reflects off a multilayer mirror at 42° and illuminates the mask at a 6° off-axis angle of incidence. This geometry allows 13.5 nm (92.5 eV) EUV in-band radiation and some longer wavelength up through visible light. Photon energies lower than the bond energies of these carbon-containing molecules are not believed to contribute to the contamination development. Carbon containing species were then injected

[a]Electronic mail: yfan@uamail.albany.edu

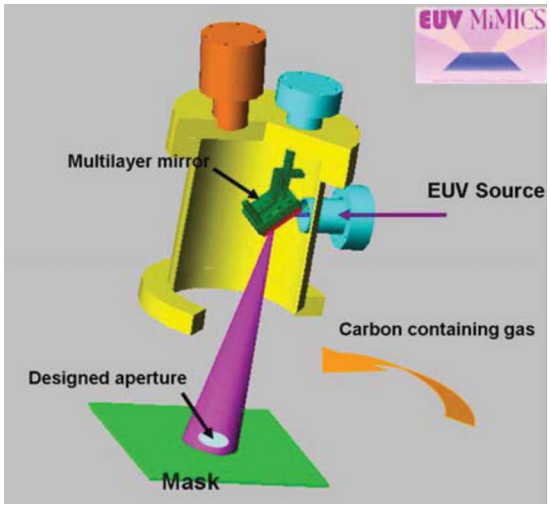

FIG. 1. (Color online) Layout of the EUV MiMICS at CNSE. Carbon containing molecules were injected into the vacuum chamber to increase the contamination rate.

into the vacuum chamber using a needle valve. A 3×5 mm^2 oval aperture was used to contaminate only those desired features within a selected area. Figure 2 illustrates a contaminated area on a patterned EUV mask.

The film stack used for this experiment was a Si-capped multilayer mirror, with SiO_2 as a buffer layer and TaN as an absorber layer. The stack contains 25 fields with different design features including 80–225 nm vertical and horizontal dense lines (16–45 nm on the wafer plane when printed in an exposure tool with a demagnification of 5). In addition to the dense 1:1 lines, the duty cycles of the lines and spaces vary from 1:4 to 4:1. Unique labels were also added for easy access and identification of each field during mask inspection.

Contamination film shown above can cause reflectivity loss, and hence the throughput loss. The reflectance change was measured using an EUV sensitive photoemission detector installed on the Berkeley MET that measures the total

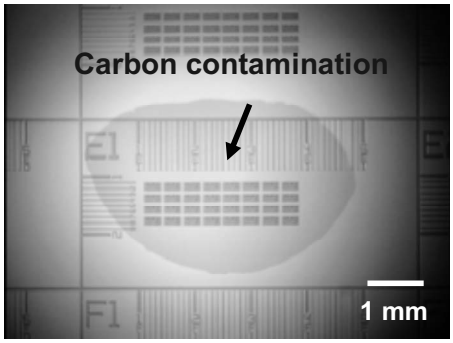

FIG. 2. 3×5 mm^2 oval aperture was designed to cause the photoinduced chemical reaction of hydrocarbons on surface within only a selected area. As shown in the optical micrograph taken by a reticle SEM, the dark oval is the carbon contamination that covers a subfield on a patterned EUV mask.

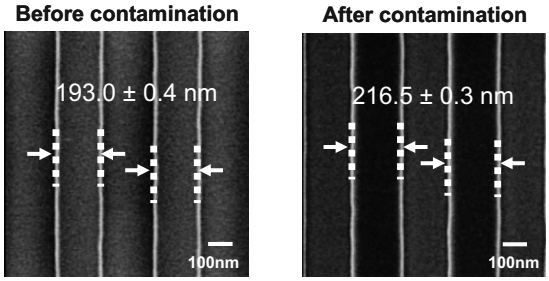

FIG. 3. Reticle SEM images show that the width of the designed 200 nm half-pitch dense lines increased by 23.5 nm after contamination.

flux of radiation coming off the mask and provides a relative reflectivity measurement for identically designed fields on the mask.

III. EXPERIMENTAL RESULTS AND ANALYSIS

Selected fields on the mask were contaminated using the EUV MiMICS tool. The background pressure in the clean chamber is 5×10^{-7} Torr, and increased to 3×10^{-6} Torr with carbon-containing gas injected. Accumulated nominal dose for a typical 8 h exposure is 5 J/cm^3 including EUV in-band and some longer wavelengths. The density of carbon was assumed to be 1.5 g/cm^3 throughout this paper based on current literature reviews from 0.8 to 2.2 g/cm^3.[6,7]

To measure the effects of carbon contamination, the change in different mask parameters was investigated as a function of carbon thickness. Mask CD, reflectivity, and surface roughness changes were monitored, and aerial analysis as well as imaging was performed.

A. Mask inspection

A top-down reticle SEM and SUMMIT software was used to record and analyze CD change on the same field before and after contamination to determine the CD variation of the absorbing features on the mask.[8] The CD was increased by 23.5 nm after an 8 h EUV exposure on 200 nm features, as shown in Fig. 3.

The CD change (labeled as ΔCD) and the reflectivity loss were measured from the selected fields on the mask and recorded in Fig. 4. We observed carbon contamination results in a reflectivity loss and ΔCD, which implies carbon deposition on the sidewalls of the absorbers. Additionally more than 95% of the field on the mask is nonpatterned area so the accuracy of reflectivity measurements from the selected fields should not be affected by the patterned region. Therefore, carbon thickness can then be calculated and shown below the reflectivity loss databased on absorption data from the Center for X-ray Optics (CXRO) and our assumption of density of carbon to be 1.5 g/cm^3.[9] This agreement also indicates that there is approximately one-half as much carbon thickness on each sidewall as on the top surface of the multilayer and absorbers.

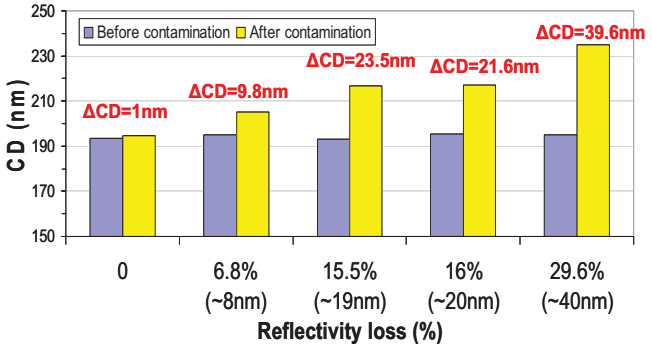

FIG. 4. (Color online) CD change (labeled as ΔCD) and the reflectivity loss were measured from selected fields on the mask, and results show that the reflectivity loss scales with the CD change, which means that there is carbon contamination on the sidewalls of the absorbers. The density of carbon was assumed to be 1.5 g/cm^3 and carbon thickness can then be calculated and shown below the reflectivity loss data. The calculated carbon thickness approximately matches the measured CD change, which indicates that there is about one-half as much carbon thickness on each sidewall as on the top surface of the multilayer and absorbers.

B. Features printing

Images were printed at the SEMATECH Berkeley MET, and the exposed wafers were analyzed using a CD-SEM. To investigate the impact of carbon contamination on printing results, selected fields on the mask were exposed to EUV radiation with the dose controlled to deposit carbon layers of different thicknesses on each field. Carbon thicknesses were determined to be 8, 19, and 40 nm, respectively, based on the CXRO data and reflectivity measurements before printing. Figures 5(a) and 6(a) show the printed images in a focus exposure matrix for both clean and contaminated regions on the mask. In terms of printing performance, Bossung plots are often used to determine the dose sensitivity and printability at various doses and focuses.[10] Results are shown in Figs. 5(b) and 6(b); each curve in the plot is the trend line of the measured CD at various dose levels. When the curves are flatter, the printing is less sensitive to focus change. Similarly, when the curves are closer to each other, the printed size fluctuates less, and thus the exposure latitude is larger. In this experiment, images printed from clean region showed a better performance than contaminated region on the mask.

Figure 7 compares, for a given field on the mask, the relative increase in dose to print 40 nm half-pitch dense lines as a function of carbon layer thickness with the relative reflectivity loss for the same carbon thickness. For instance, with 19 nm thick carbon, the dose increased more than 45% while the reflectivity loss was only 16%. This result indicates that the dose change depends not only on the carbon thickness, and hence the reflectivity loss on the mask surface, but also on the topography of the contaminated features.

C. Surface analysis

A Veeco Dimension 3100 AFM with a high aspect ratio focused ion beam tip was used in tapping mode for surface topography measurements. The full width at half maximum (FWHM) for the contaminated features was observed to increase from 234.8 to 275.4 nm, which was a 40.6 nm CD change with 19 nm of carbon deposited on the selected fields of the EUV mask, as shown in Fig. 8. This is an indication of contamination topography that appears to be conformal, nevertheless cross-sectional measurement of contaminated features is still needed in order to estimate the effects of carbon contamination accurately. The root mean square (rms) roughness of the contaminated region was measured to be 0.45 nm as compared to 0.29 nm in a clean area. The increase in rms roughness can cause more flare during exposure and could be a potential cause of line edge roughness on the printed images.[11]

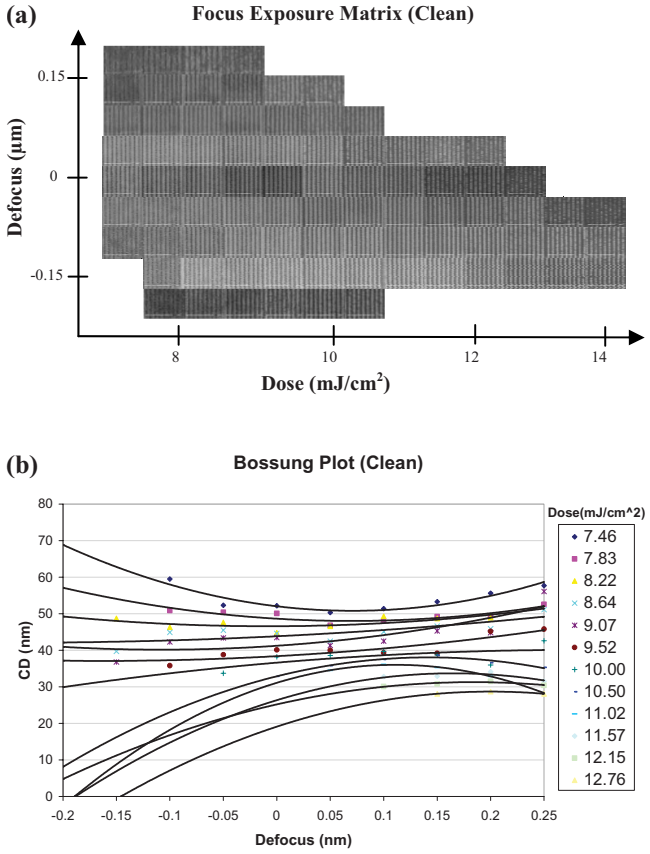

FIG. 5. (Color online) Focus exposure matrix shown in (a) represents the printability at various doses and focuses. Trend lines of measured linewidth, or so called Bossung plots, are also shown in (b). With 5% dose steps, the exposure latitude across ±10% CD variation was 30% at best focus.

D. Aerial image analysis

The SEMATECH Berkeley AIT was used to inspect the contaminated mask and record aerial images. The recorded images underwent through-focus behavior aerial image data analysis and processing, such as CD measurement, contrast curve, normalized image log slope, linewidth roughness, and process window using THROUGHFOCUS software.[12] Figure 9 compares 200 nm dense lines on both clean and contaminated regions of the mask, and recorded as aerial image profiles in Fig. 10. The thickness of the deposited carbon on the contaminated mask was 19 nm after EUV exposure with a 5 J/cm^2 of nominal dose in the MiMICS tool.

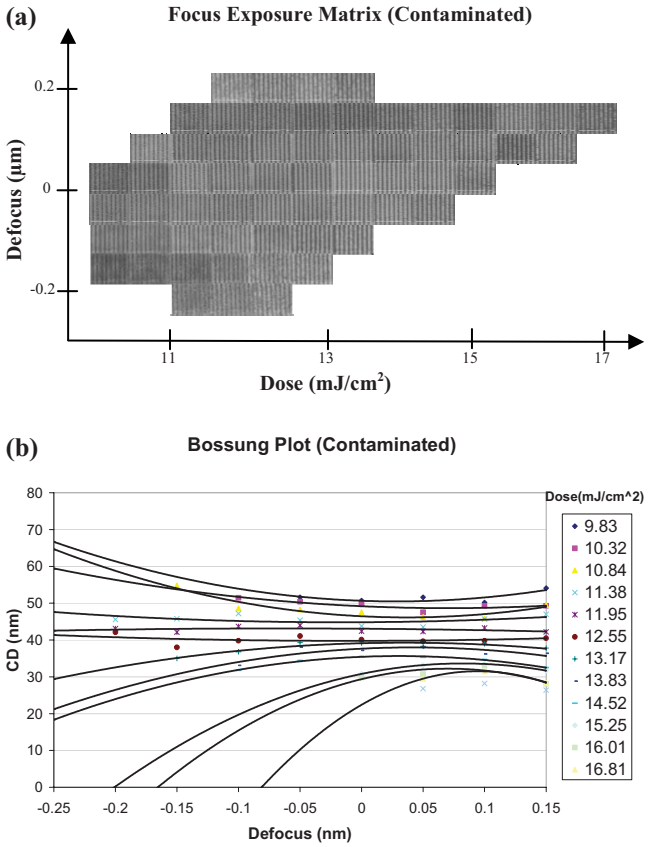

FIG. 6. (Color online) Focus exposure matrix in (a) had worse printability than images printed at the clean region on the mask. From the Bossung plot shown in (b), the best dose to print a 40 nm target CD is ~12.55 mJ/cm^2, which is about 21% more than the best dose to print the clean region on the mask with 8 nm of carbon deposited. The exposure latitude across ±10% CD variation is 25% at best focus.

In through-focus image analysis, data were processed using mask units since all the aerial images were recorded from a mask. As shown in Fig. 11(a), Bossung curves were calculated to determine CD versus focus at 5% dose steps (threshold) to estimate the maximum tolerance of dose change to print within a ±10% CD variation.[10] Contrast, normalized image log slope (NILS) and linewidth roughness (LWR) 3σ through focus were calculated, as shown in Figs. 11(b)–11(d). By all these methods of evaluation, clean regions on the mask showed a better performance than the contaminated regions.

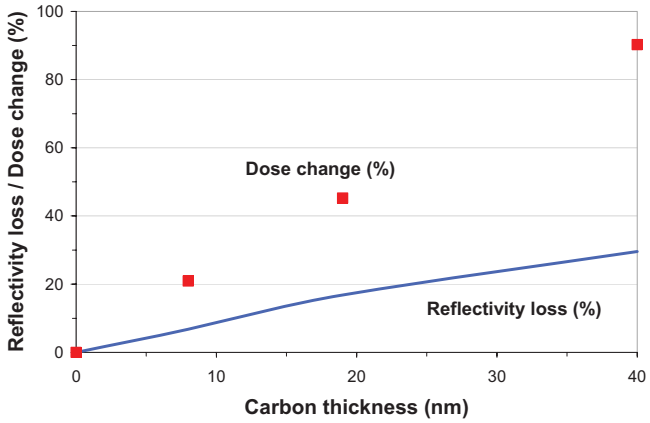

FIG. 7. (Color online) Required dose change to print dense lines vs carbon thickness is plotted and compared to the measured reflectivity loss on the selected fields of the mask. Carbon thicknesses were determined using absorption data from the CXRO website.

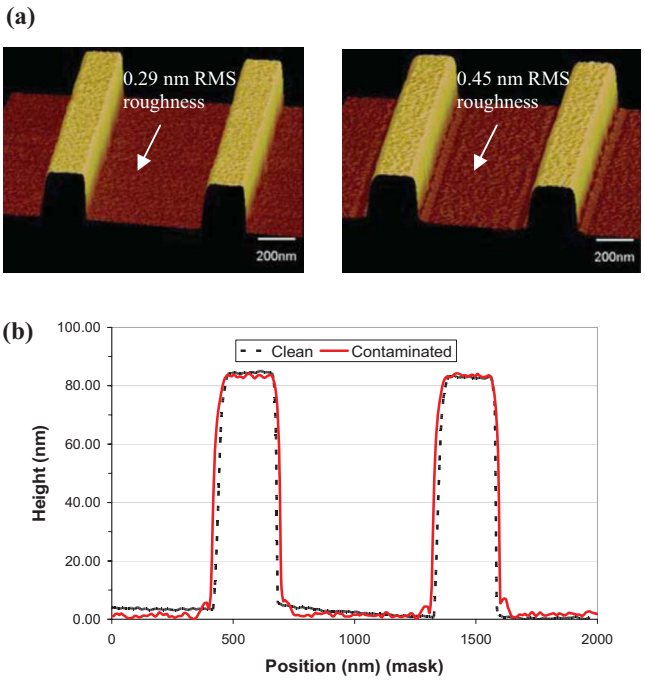

FIG. 8. (Color online) (a) 3D computer images of surface morphology were created based on surface scan using an AFM. Features shown are 225 nm lines and 675 nm spaces (1:3 lines/spaces ratio). rms roughness on a clean mask was 0.29 nm, which increased to 0.45 nm on a contaminated region on the mask. (b) FWHM of 225 nm lines and spaces features was measured on the mask. The sidewall of the absorber increased by 40.6 nm for the contaminated features.

IV. SIMULATION OF CONTAMINATION TOPOGRAPHY

A. Model development

EM-SUITE, lithographic software developed by Panoramic Technology Inc., was used to investigate the change in topography of a patterned EUV mask due to carbon contamination. EM-SUITE can calculate the intensity reflected off a mask based on a finite difference time domain algorithm.[13,14]

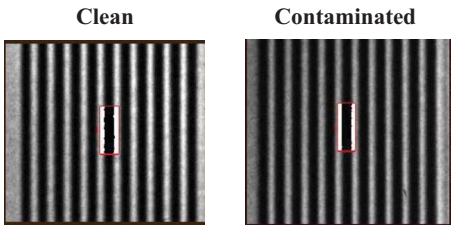

FIG. 9. (Color online) Aerial images recorded using the SEMATECH Berkeley AIT show 200 nm dense line features on the mask for the clean and contaminated areas. The 0.5×2 μm^2 boxes shown were selected for data analysis.

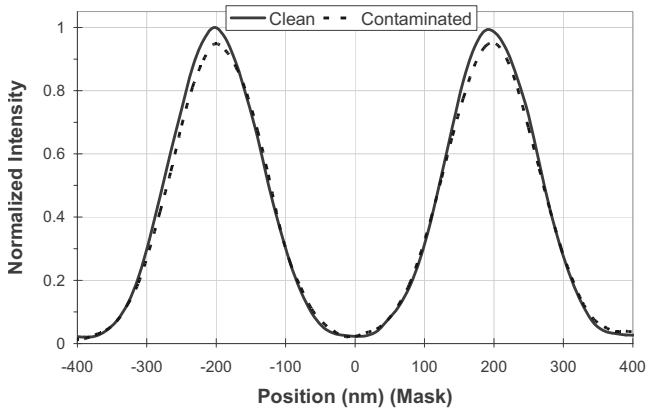

FIG. 10. Intensity profile was recorded based on the location of imaging processing on the mask. Results show less contrast is recorded from the contaminated region on the mask.

The film stack used for both the printing experiments and simulations was typical of an EUV mask, a Si-capped Mo/Si multilayer mirror, with 10 nm SiO_2 as a buffer layer and 67 nm TaN as an absorber layer. The feature size used for both features printing and simulation was 200 nm dense lines on the mask. In this simulation, optical parameters were 0.25 numerical aperture (NA), 6° angle of incidence, and 0.5 sigma partial coherence illumination as the specifications to match the ASML alpha demo tool (ADT).[15]

Sigma (σ) is defined in the following:

$$\sigma = \frac{\mathrm{NA}_C}{\mathrm{NA}_O}, \tag{1}$$

where NA_C is the condenser lens NA and NA_O is the objective lens NA. The optics were assumed to be aberration-free and the multilayer stack of the mask is defect-free.

It is not yet clear whether the growth rate of carbon deposition will be dependent on the exposed material, such as TaN absorber versus Si or Ru capped multilayer. However, the absorber topography and the illumination angles can still cause different carbon deposition rates between the top surfaces and the sidewalls of the absorbing features. Two extreme cases of possible topography were considered, either direct deposition or conformal topography, as shown in Fig. 12. Both conformal and direct carbon depositions cause a reflectivity drop due to the absorption of EUV radiation, but the carbon growth on the sidewall in conformal topography causes a larger increase in CD than direct deposition.

Another factor one should concern is the shadowing effect due to the oblique illumination of EUV radiation, as shown in Fig. 13, and can cause CD error when printing different features on EUV masks, and hence results in horizontal-vertical (*H-V*) bias. In addition, carbon contamination can make the shadowing effect even worse due to the contaminated sidewall of absorbers. In order to solve this issue, an optical correction was applied. For a clean mask, a 5 nm *H-V* bias between shadowed and nonshadowed illuminations was calculated for identical feature sizes at the same exposure dose. Therefore, in the simulations, a CD compensation was applied on the clean mask to correct for this *H-V* bias. Then, further calculations were performed on the compensated mask, including carbon contamination, to see whether the compensation was effective and accurate.

Compared to the ASML ADT, the SEMATECH Berkeley MET uses a different optics designs,[5] and optical parameters are 0.3 NA, 4° angle of incidence, and an annular illumination with sigma of 0.35–0.55 were used. The variations in the exposure tool and simulations were compared and shown in Fig. 14 with 40 nm target CD printed. The ASML ADT requires more doses to print mainly due to the larger angle of instance, and hence the lower intensity reflected off the EUV mask.

B. Simulation results

To understand whether our assumptions matched the experimental data, aerial images and calculated resist parameters were compared to the printed results. As shown in Fig. 15, the experimental data of 40 nm target CD for both nonshadowed and shadowed cases fall between the two extreme cases, direct and conformal depositions. This indicates that the actual topography of the carbon contamination could be a combination of the two. More importantly, conformal deposition requires more than 45% more dose than the direct deposition to reach the target CD, for 19 nm of carbon deposited on the mask. This has also been seen in printing experiments, which could indicate that the contamination topography affects the imaging significantly.

As the calculations show in Fig. 15 for both conformal and direct depositions, the *H-V* bias is noticeable and increases as more carbon deposits on the mask. In addition, conformal deposition leads to a larger *H-V* bias than direct deposition. For a clean mask, a 5 nm CD compensation was applied to correct for this *H-V* bias. As shown in Fig. 16, which depicts the conformal deposition with the greatest *H-V* bias, the compensation works well when the carbon layer is thin. However, when the carbon thickness is greater than 10 nm, the *H-V* bias appears again, and the dose change for this carbon growth is 2%. More importantly, there are still some factors one should take into account to achieve the maximum allowed ±10% CD variation for HVM tools, such as line edge roughness and optical aberrations. This means that the accuracy of the CD compensation could still fail for 40 nm dense lines on the wafer when more carbon is present.

In actual HVM exposure tools, smaller features, various duty cycles, or unwanted effects such as optical aberrations, could make this effect more noticeable even when the carbon layer is thinner. Carbon mitigation has been studied and used to reduce the contamination effect on multilayer surfaces;[7,16] however, the removal of the contamination on patterned EUV masks needs more study since the absorbing features can be damaged and affect the lifetime of the mask during the carbon mitigation process.

V. CONCLUSION

The lifetime of EUV optics and masks is critical to move EUV lithography from development to HVM. One of the

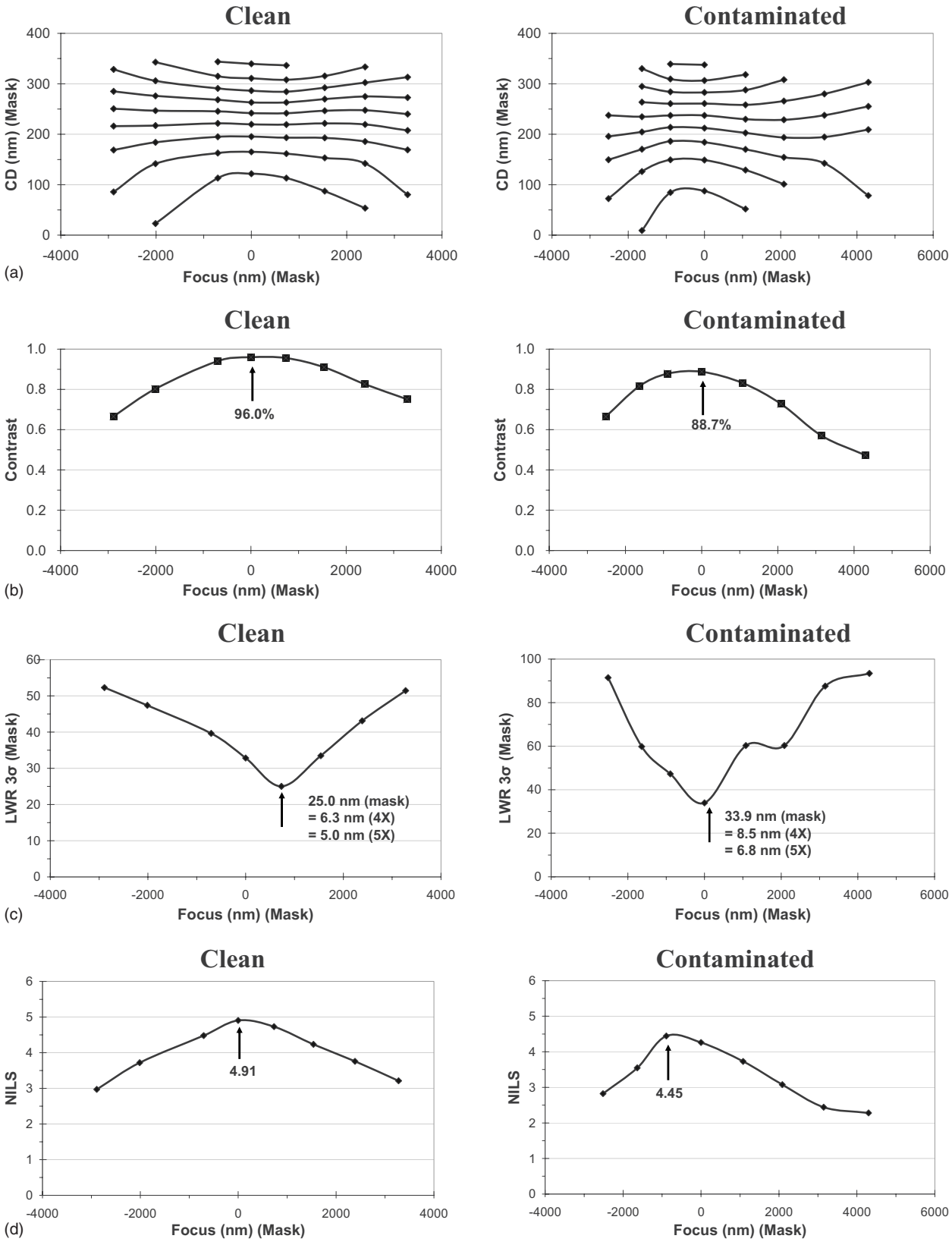

FIG. 11. (a) CD through focus showed the normalized intensity at different threshold levels from 0.1 to 0.9, spaced by 0.1. The CD change at best focus for clean region on the mask was increased from 218 to 250 nm after contamination. (b) Contrast through focus is calculated at a 200 nm 1:1 lines/spaces region on the mask. (c) LWR 3σ was shown above at 1:1 intensity on the mask. Equivalent sizes for $5\times$ demagnification are also shown. (d) NILS was determined at the best focus for each field. The larger NILS, the better image quality of printed features, and the clean region had a 10% larger NILS than the clean region.

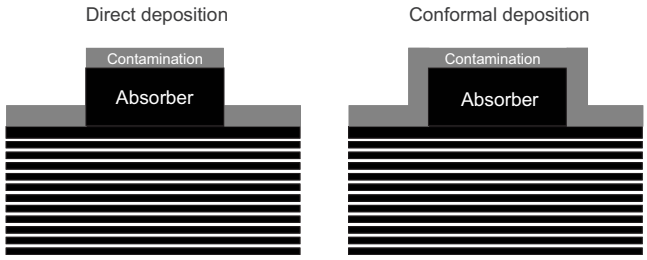

FIG. 12. Two possible topographies: direct and conformal deposition. The film stack used in the simulation consisted of 40 bilayers of Mo/Si, 10 nm of SiO_2 as a buffer layer, and 70 nm of TaN as an absorber layer. The gray layer shown in the schematic view represents the deposited carbon layer.

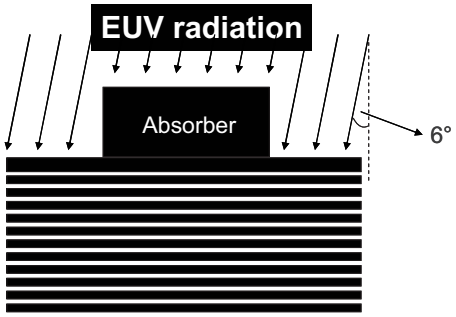

FIG. 13. Shadowing effects occurs on patterned masks when EUV radiation is perpendicular to the absorbers.

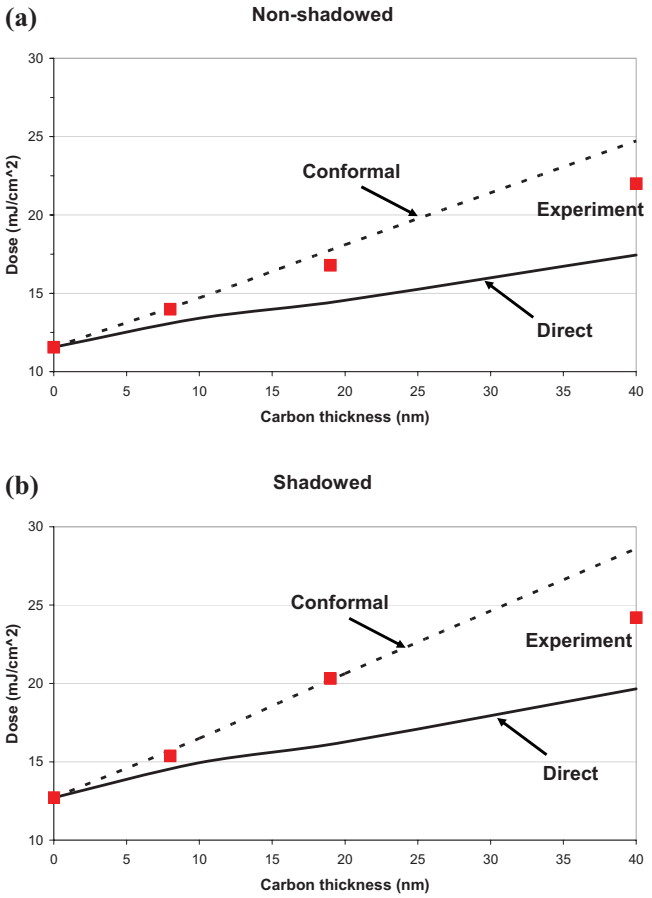

FIG. 15. (Color online) Simulations of dose required to print 40 nm target CD were performed for conformal and direct carbon topography, as well as shadowed and nonshadowed illumination conditions. The experimental results fall between the conformal and direct topographies for both the shadowed and nonshadowed illumination conditions.

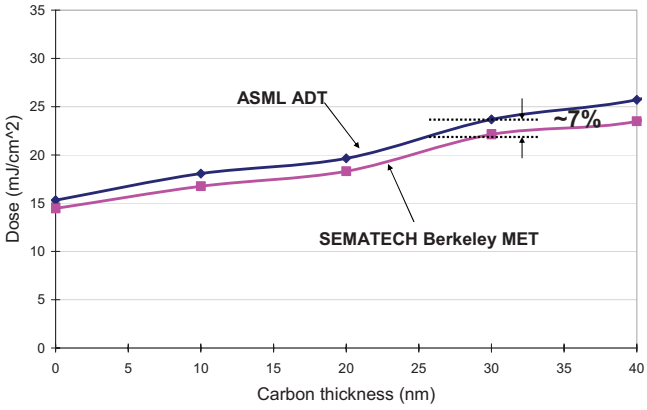

FIG. 14. (Color online) Simulations of the dose required to print 40 nm target CD were performed for both the ASML ADT and the SEMATECH Berkeley MET. The difference in optical designs between these two tools led to a 7% difference in dose required to print these features.

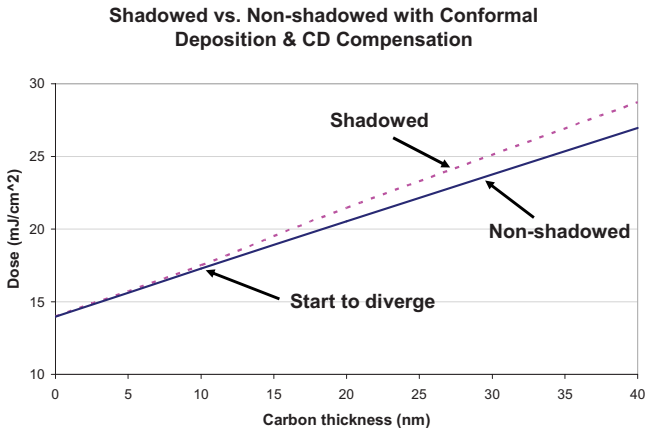

FIG. 16. (Color online) Plot of the dose required to print the target CD of 40 nm dense lines on the wafer. With increasing carbon thickness, a larger dose is required and the divergence of the dose curves for shadowed and nonshadowed cases increases.

lifetime issues for EUV masks is EUV-induced carbon contamination. In this work, selected fields on the mask were contaminated and inspected using a top-down SEM and an AFM. Results showed CD changes from contaminated regions on the mask, which indicated the carbon layer also deposited on the sidewall of the absorbers. Due to the oblique illumination in EUV exposure tools, the sidewall contamination causes extra loss of EUV radiation than a simple absorption model. This was also verified by printing experiments. The required dose was increased dramatically by 45% when 19 nm of carbon was deposited. Assuming that the maximum loss of throughput that the industry can tolerate is 5%, then only 2.5 nm of carbon contamination is allowed. Although the contamination rate in each exposure tool will be different, it is still likely to fall short of the industry goal of 30 000 h lifetime for EUV optics and masks.[17]

Aerial image analysis was used to understand the effects of carbon contamination on imaging. Simulations were also performed with both direct and conformal depositions to compare with the experimental data. Preliminary simulation results showed that the maximum allowed contamination was 10 nm before CD compensation failed. However, the prediction on printing performance can be improved only if the actual topography of carbon contamination is known.

To date, researchers are investigating various techniques to minimize the effects of carbon contamination on EUV optics, such as different capping layers and atomic hydrogen cleaning.[17,18] For patterned EUV masks, less work has been completed. Direct measurement of the contamination topography is still a challenge and more work is needed to provide sufficient data before EUV lithography is ready for HVM.

ACKNOWLEDGMENTS

The author would like to thank Paul Denham, Gideon Jones, Brian Hoef, and Lorie-Mae Baclea-an from Berkeley MET team for great help. Financial support from SEMATECH is also gratefully acknowledged.

[1]Y. Fan *et al.*, Proc. SPIE **7271**, 72713U (2009).
[2]G. Denbeaux, International Workshop on EUV Lithography, Hawaii, 2009.
[3]P. Blackborow, M. Partlow, S. Horne, M. Besen, D. Smith, and D. Gustafson, Proc. SPIE **6921**, 692121 (2008).
[4]K. Goldberg, S. Rekawa, C. Kemp, A. Barty, E. Anderson, P. Kearney, and H. Han, Proc. SPIE **6921**, 69213U (2008).
[5]P. Naulleau *et al.*, Proc. SPIE **5374**, 881 (2004).
[6]J. Hollenshead and L. Klebanoff, J. Vac. Sci. Technol. B **24**, 64 (2006).
[7]Y. Nishiyama, T. Anazawa, H. Oizumi, I. Nishiyama, O. Suga, K. Abe, S. Kagata, and A. Izumi, Proc. SPIE **6921**, 692116 (2008).
[8]See: http://www.euvl.com/summit/.
[9]See: http://www.cxro.lbl.gov/.
[10]J. W. Bossung, Proc. SPIE **100**, 80 (1977).
[11]H. Tanabe, G. Yoshizawa, Y. Liu, V. Tolani, and K. Kojima, N. Hayashi, Proc. SPIE **6607**, 66071H (2007).
[12]See: http://ThroughFocus.com.
[13]See: http://www.panoramictech.com/.
[14]T. Pistor, "Expanding the simulation capability of TEMPEST," M.S. thesis, University of California, 1997.
[15]H. Meiling *et al.*, Proc. SPIE **6151**, 615108 (2006).
[16]S. Huh *et al.*, Proc. SPIE **6921**, 692115 (2008).
[17]S. Bajt, and V. Bakshi, "Optics Contamination," *EUV Lithography* (SPIE and Wiley and Sons, New York, 2009), pp. 227–259.
[18]H. Oizumi *et al.*, Jpn. J. Appl. Phys., Part 1 **46**, L633 (2007).